DRYING TECHNOLOGY, 20(5), 1239–1267 (2002)

DESIGN AND TESTING OF A NEW SOLAR TRAY DRYER

N. A. Vlachos,[1] T. D. Karapantsios,[1,2,*] A. I. Balouktsis,[3] and D. Chassapis[3]

[1]Department of Food Technology, Technological Educational Institution of Thessaloniki, P.O. Box 14561, 541 01, Thessaloniki, Greece
[2]Department of Chemistry, Chemical Technology Division, Aristotle University of Thessaloniki, (Box 116), 540 06 Thessaloniki, Greece
[3]Department of Mechanical Engineering, Technological Educational Institution of Serres, End of Magnesia's str., GR-62 100 Serres, Greece

ABSTRACT

A novel low cost tray dryer equipped with a solar air collector, a heat storage cabinet and a solar chimney is designed and tested. The design is based on energy balances and on an hourly-averaged radiation data reduction procedure for tilted surfaces. Measurements of total solar radiation on an horizontal plane, ambient temperature and humidity, air speed, temperature and relative humidity inside the dryer as well as solids moisture loss-in-weight data are employed as a means to study the performance of the dryer. First, detailed

*Corresponding author. Fax: +30-310-99 7759; E-mail: karapant@chem.auth.gr

diagnostic experiments are carried out with no drying material on the trays. Next, a number of experiments is conducted using a controlled reference material whose reproducible dehydration pattern allows comparisons among runs. Drying is also tested during night operation and under adverse weather conditions. For all the employed conditions, the material gets completely dehydrated at a satisfactory rate and with an encouraging system's efficiency.

Key Words: Heat storage; Night operation; Solar air collector; Solar chimney; Solar drying; Weather conditions

INTRODUCTION

Solar drying refers to a technique that utilizes incident solar radiation to convert it into thermal energy required for drying purposes. According to Ratti and Mujumdar (1997), solar-energy drying, where feasible, often provides the most cost-effective drying technique. Ekechukwu and Norton (1999), in reviewing the various designs of solar-energy drying systems, classified them with respect to their operating temperature ranges, heat supply modes and sources, operational modes and structural modes as well. Natural-circulation and forced-convection solar dryers are the two main groups that were identified. As regards their structural arrangement three generic subclasses were also identified: direct-modes (the solar-energy collection unit is an integral part of the entire drying system), indirect-modes (the solar collector and the drying chamber are separate units) and mixed-modes solar dryers.

For many agricultural products an abrupt drying process is completely undesirable, since it demotes the product's quality and the final drying result seems to be uncontrollable. This is due to the fact that quite often an external over-dried layer is formed which prohibits the process of drying at the material's inner layers. On the other hand, the rather slow process of direct (also called open) sun drying, a traditional drying technique in Mediterranean climates where high solar irradiation occurs, can have a negative impact on dried products' quality mainly due to contamination, e.g. by windborne dirt and dust, insects etc. The resulting decrease in quality renders the product less marketable (Tiris et al., 1994). In addition to this, rainfall can even destroy the whole drying process. However, the main drawback of direct sun drying is the lack of process control and treatment uniformity (e.g. Bansal and Garg, 1987; Garg, 1987; Barbosa-Canovas and Vega-Mercado, 1996 etc.). In such conditions, indirect solar dryers appear to be an appropriate alternative proposition.

Several types of indirect solar dryers were realized and built in the past, aiming to products of higher quality in terms of color, texture or taste, reduced drying times and greater efficiencies compared to the traditional open sun drying (e.g. Imre, 1987; Das and Kumar, 1989; Tsamparlis, 1990; Imre et al., 1990; Tiris et al., 1994; Pratoto et al., 1997; Esper and Muhlbauer, 1998; Arinze et al., 1999; Bala and Mondal, 2001). When designing such dryers, the cost of construction and the range of applicability are two additional factors that pose an even greater challenge in developing an economically viable drying system. Therefore, for a Mediterranean country like Greece where solar radiation is abundant, the idea of designing a low cost and high performance drying system appears tempting.

The primary objective of this study is to design, construct and evaluate a small-scale tray dryer furnished with a solar air heater, a solar chimney and a heat storage cabinet. The dryer is built up in the city of Serres (latitude $41^\circ 07'$, longitude $23^\circ 34'$, altitude 32 m), the capital of a large rural prefecture of Greece. Initial tests with popular agricultural products of the area (rice and tobacco) as drying materials did not permit the accurate depiction of the dryer's performance due to variations of product conditions (moisture content, bed porosity etc.). For this reason a reference drying material is employed instead.

The performance of the dryer is tested also under adverse weather conditions (i.e. cloudy and rainy) and during night operation. In this respect, the recent studies by Ekechukwu and Norton (1998) and Aboul-Enein et al. (2000) are of particular interest to the present work. The former authors studied the effect of seasonal weather variations on a solar-assisted crop dryer and concluded that wet season drying conditions were considerably more unpredictable and resulted in poorer drying compared to drying under dry season conditions. Aboul-Enein et al., studied the operation of a solar-assisted dryer extended through the night hours and found that thermal storage during the day can be used as a heat source during the night for continuing the drying of agricultural products and also preventing their re-hydration from the surrounding air.

In the following section, a comprehensive design scenario for the dryer is presented. Subsequently, the dryer set-up and its operation are outlined. Finally, the experiments carried out in this work and the main results are presented and discussed.

DESIGN CONSIDERATIONS

An indirect solar dryer consists of three major components. The solar collector where the ambient air preheats, the drying chamber where the material to be dried comes in direct contact with the hot air from the collector and reduces its moisture and, finally, the solar chimney which promotes the air lift through the dryer. In the analysis below, we assume that the incident solar radiation is sufficient to bring the dryer's body to its steady state temperature and also to counterbalance heat losses. Then, the *batch* energy balance in the drying chamber becomes (e.g. Jansen, 1985; Das and Kumar, 1989):

$$V_a\rho_a[c_{\mathrm{pa}}(T_{\mathrm{oc}}-T_{\mathrm{od}})+\lambda(y_{\mathrm{oc}}-y_{\mathrm{od}})] \\ =\frac{W}{t}\{(m_i-m_f)[\lambda+c_{\mathrm{pw}}(T_{\mathrm{od}}-T_{\mathrm{am}})]+c_{\mathrm{ps}}(T_{\mathrm{od}}-T_{\mathrm{am}})\} \tag{1}$$

V is the volumetric flow rate (m^3/h), ρ is the average density (kg/m^3), c_p is the average heat capacity (kJ/kgK), λ is the average latent heat of water (kJ/kg), y is the absolute humidity of air (kg H_2O/kg dry air), T is the temperature ($^\circ$C), W is the weight of dry solid (kg), m is the solid's moisture content (kg H_2O/kg dry solid) and t is the drying period (h). Accordingly, subscripts denote the following; *a*: air, *w*: water, *s*: solid, oc: exit from collector, od: exit from drying chamber, am: ambient, *i*: initial, *f*: final.

The air density is related to air temperature and absolute humidity according to the following (Oosthuizen, 1987):

$$\rho_a=\rho_o\left[\frac{1}{(1+T/273)}\right](1+y) \tag{2}$$

where ρ_o the air density at $T=273$ K (=1.293 kg/m^3). The second term of the LHS of Eq. (1) describes the change of the air energy associated with the moisture uptake. In most usual cases this term is small and can be safely ignored.

Neglecting any parasitic energy delivered to the dryer, e.g., from an electrical fan, the solar air collector operation is described by:

$$[I_T(\tau\alpha)_e-U_L(T_p-T_{\mathrm{am}})]A_c=(V_a\rho_a c_{\mathrm{pa}})(T_{\mathrm{oc}}-T_i) \tag{3}$$

where A_c is the collector area (m^2), I_T is the insolation rate per unit area on the collector's tilted plane (W/m^2), $(\tau\alpha)_c$ is the effective absorbance-transmittance product (dim/less), U_L is the collector's overall heat loss coefficient (W/m$^{2\circ}$C), T_ρ is the average temperature of the collector's plate and T_i is the temperature of the air entering the collector. The transmittance of the glazing, τ, has a value around 0.85 and the absorbance of the black painted plate, α, is around 0.95, while in most usual situations U_L is close to 5 W/m$^{2\circ}$C (Garg, 1987).

To overcome the difficulty of accurately determining T_ρ in Eq. (3), the collector heat removal factor, F_R, is introduced and we end up with the Hottel-Whillier-Bliss equation:

$$F_R[I_T(\tau\alpha)_e - U_L(T_i - T_{\mathrm{am}})]A_c = (V_a \rho_a c_{\mathrm{pa}})(T_{\mathrm{oc}} - T_i) \tag{4}$$

For air heating collectors, F_R, is around 0.7 (Garg, 1987). Since the collector is fed directly with ambient air, T_i equals T_{am} and so the second term on the left-hand side vanishes and the rate of energy collection is simply:

$$A_c F_R I_T(\tau\alpha)_e = (V_a \rho_a c_{\mathrm{pa}})(T_{\mathrm{oc}} - T_{\mathrm{am}}) \tag{5}$$

The major problem in the design of solar-assisted dryers is that I_T is not known for most sites. Instead, what is traditionally recorded in meteorological stations is I, the solar radiation received on an horizontal plane. Lalas et al. (1982) presented extended tabulations with their model predic- **AQ1**
tions of solar radiation on tilted surfaces, for many sites in Greece, based on measurements of horizontal radiation. These predictions, however, are verified only by comparison against data from a single site (Athens, Greece) and furthermore, are over twenty years old. In the last decade, the meteoclimatic conditions in the region of Greece have changed considerably (Karapantsios et al., 1999). Therefore, in order to deduce I_T from available local measurements of solar radiation on an horizontal plane, a general procedure is employed. The relations below, unless differently stated, are taken from Duffie and Beckman (1991).

The total solar radiation on an horizontal plane, I, is customary expressed as the sum of two components: the beam (or direct) radiation and the diffuse radiation from the sky:

$$I = I_b + I_d \tag{6}$$

Assuming hourly average radiation values, the clearness index k_T is defined:

$$k_T = \frac{I}{I_o} \tag{7}$$

where I_o is the extraterrestrial radiation on an horizontal plane given as:

$$I_o = \frac{12 \times 3600}{\pi} G_{\mathrm{sc}} \left(1 + 0.033 \cos \frac{360n}{365}\right) \times \left[\cos\phi \cos\delta (\sin\omega_2 - \sin\omega_1) + \frac{\pi(\omega_2 - \omega_1)}{180} \sin\phi \sin\delta\right] \tag{8}$$

where G_{sc} is the solar constant (1367 W/m^2), n is the day of the year (1 to 365), ϕ is the latitude of the site (angular location from the equator), δ is the declination (angular position of the sun at solar noon) and ω is the hour angle (angular displacement of the sun east or west from the local meridian). AQ2

The declination δ is found from the equation of Cooper as cited by Duffie and Beckman (1991):

$$\delta = 23.45 \sin\left(360 \frac{284 + n}{365}\right) \tag{9}$$

whereas ω is given in degrees (negative before noon and positive after noon) by the relation:

$$\omega = 0.25^{*}(\text{minutes of the hour from local meridian}) \tag{10}$$

and the solar time, Sot (in min), is related to the standard time, Stt (in min), by:

$$\begin{aligned} \text{Sot} - \text{Stt} = 229.2(&0.000075 + 0.001868 \cos X - 0.032077 \sin X \\ &- 0.014615 \cos 2X - 0.04089 \sin 2X) \end{aligned} \tag{11}$$

where $X = (n-1)$ (360/365).

The diffuse radiation component is evaluated next from the following correlation:

$$\frac{I_d}{I} = \begin{cases} 1.0 - 0.09\, k_T & \text{for } k_T \le 0.22 \\ 0.9511 - 0.1604\, k_T + 4.388\, k_T^2 & \\ \quad -16.638\, k_T^3 + 12.336\, k_T^4 & \text{for } 0.22 < k_T \le 0.80 \\ 0.165 & \text{for } k_T > 0.80 \end{cases} \tag{12}$$

and from that the direct radiation component is computed as:

$$I_b = I - I_d \tag{13}$$

A customary approach for radiation estimations on sloped surfaces is to consider an isotropic model for the diffuse radiation (Liu and Jordan, 1963) and also assume that the reflecting surfaces are diffuse and not specular reflectors. In this case, the radiation on the collector's surface tilted at slope β, is given by (Sukhatme, 1984): AQ3

$$I_T = I_b R_b + I_d\left(\frac{1 + \cos\beta}{2}\right) + I r_g\left(\frac{1 - \cos\beta}{2}\right) \tag{14}$$

where the last term on the RHS describes the radiation reflected from the various surfaces "seen" by the collector, r_g is the diffuse reflectance of the surroundings (usually around 0.20) and R_b is the ratio of beam radiation on the tilted surface to that on the horizontal plane. R_b for the northern hemisphere is given by (Sukhatme, 1984): AQ3

$$R_b = \frac{\cos(\phi - \beta)\cos\delta\cos\omega + \sin(\phi - \beta)\sin\delta}{\cos\phi\cos\delta\cos\omega + \sin\phi\sin\delta} \tag{15}$$

Table 1 presents calculated results of monthly average hourly values of I_T/I for August and September 2000 (the period of the tests) and for certain collector inclinations of practical interest based on horizontal radiation data recorded at the meteorological station in TEI. The table also includes monthly average daily values, H_T/H, of the same quantity throughout the years 1997–2000. The small discrepancy between the average daily H_T/H values for August and September 1997–2000 and those summed up from hourly I_T/I values in 2000 is due to the variance of solar radiation even among neighboring years. T1

Given the I_T values and for prescribed values of t, W, m_i and m_f, the usual design variables of the dryer are A_c, V_a and T_{od}, since T_{oc} is normally defined a priori not to exceed a certain temperature in order to avoid deterioration of the material's quality. Assuming the dryer's body has reached a steady state temperature before the material is introduced and also neglecting heat losses, then the minimum collector area required to evaporate the certain amount of moisture is given by equating the LHS of Eq. (5) to the RHS of Eq. (1), where also $T_{\mathrm{od}} \approx T_{\mathrm{am}}$. In this case, A_c can be calculated as:

$$A_c = \frac{W(m_i - m_f)\lambda}{F_R(\tau\alpha)_e \int_0^t I_T\,dt} \tag{16}$$

where the collector's area is estimated not instantaneously but as a function of the long-term system performance by integrating over a period of time. For the needs of the present simulation, we set $t = 8\,\mathrm{h}$, which warrants an adequate duration of daylight even in wintertime. As soon as A_c is in hand, one can determine, V_a from Eq. (5):

$$V_a = \frac{A_c F_R(\tau\alpha)_e \int_0^t I_T\,dt}{\rho_a c_{\mathrm{pa}}(T_{\mathrm{oc}} - T_{\mathrm{am}})} \tag{17}$$

Here it is taken $T_{\mathrm{oc}}^{\max} = 50^\circ\mathrm{C}$ in order to ascertain slow drying. Figure 1 displays the results of the simulation for 30°, 45° and 60° collector inclination and for all the months of the year. Calculations employ monthly F1

Table 1. Monthly Average Hourly Values of I_T/I for August and September 2000 and Monthly Average Daily Values of H_T/H Throughout the Years 1997–2000 for 30°, 45° and 60° Collector Inclination, Calculated from Meteorological Data Measured in TEI (Serres)

Hours of the Day, Standard Time	I_T/I, Monthly Average Hourly Values: August 2000			September 2000				H_T/H, Monthly Average Daily Values (1997–2000)		
	30°	45°	60°	30°	45°	60°	Month	30°	45°	60°
							Jan	1.51	1.66	1.71
7–8	0.91	0.86	0.73	1.04	1.00	0.97	Feb	1.32	1.38	1.38
8–9	0.98	0.89	0.76	1.10	1.04	0.98	Mar	1.17	1.16	1.11
9–10	1.03	0.96	0.84	1.13	1.10	1.01	Apr	1.03	0.96	0.87
10–11	1.05	1.00	0.89	1.15	1.13	1.05	May	0.94	0.84	0.72
11–12	1.08	1.02	0.92	1.16	1.15	1.08	June	0.90	0.79	0.66
12–13	1.08	1.03	0.93	1.16	1.15	1.08	July	0.92	0.81	0.68
13–14	1.07	1.02	0.91	1.16	1.15	1.07	Aug	1.00	0.92	0.81
14–15	1.05	0.99	0.88	1.15	1.14	1.06	Sept	1.13	1.11	1.03
15–16	1.02	0.96	0.84	1.13	1.10	1.03	Oct	1.30	1.35	1.33
16–17	0.93	0.89	0.74	1.10	1.06	0.97	Nov	1.48	1.60	1.65
17–18	0.86	0.77	0.61	1.04	0.95	0.90	Dec	1.55	1.70	1.77

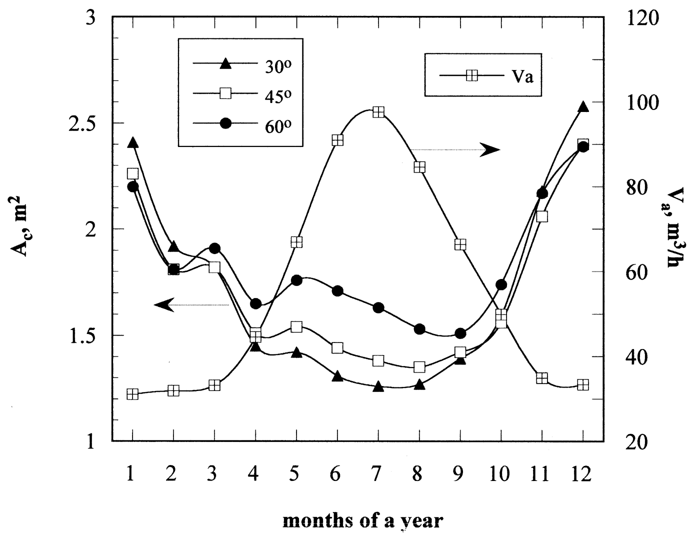

Figure 1. Simulation results regarding the collector's area, A_c, and the air volumetric flow rate, V_a, for 30°, 45° and 60° collector inclination, employing meteorological data measured in TEI (Serres).

average hourly values of solar radiation and ambient temperature recorded in TEI. The simulation is performed for a 5 kg load of material dehydrated from 85% to 0% (w.b.) moisture content. It can be seen that A_c varies approximately between 1.2 and 2.6 m^2 whereas V_a between 30 and 100 m^3/h, depending on the climatic conditions. The variation of V_a actually reflects the different average ambient temperatures among months.

In a real application, however, the diurnal variation of solar radiation (within the 8 h of drying) leads to a particularly time dependent V_a, a fact that greatly complicates the evaluation of the dryer's performance. Moreover, V_a depends significantly on the hydrodynamics of air flow and is actually dictated by the pressure drop through the dryer (collector-drying chamber-chimney). Thus, a more elaborate analysis would involve the momentum equation across different sections of the dryer but this requires an accurate knowledge of the geometrical details of the whole setup and is beyond the scope of the present work. Therefore, for the experimental testing of the dryer, V_a is maintained constant (by employing an electrical fan) at a sufficient level (200 m^3/h) which, even during peak insolation, maintains the collector outlet temperature below the maximum drying temperature, $T_{oc}^{max} = 50°C$.

Finally, the collector's efficiency is determined by:

$$E_c = \frac{V_a \rho_a c_{pa} \int_0^t (T_{oc} - T_{am})\, dt}{A_c \int_0^t I_T\, dt} \tag{18}$$

A measure of the drying efficiency (after the collector) is the ratio of the energy required to evaporate moisture from the product to the energy supplied to the dryer:

$$E_d = \frac{W(m_i - m_f)\lambda}{A_c F_R(\tau\alpha)_e \int_0^t I_T\, dt} \tag{19}$$

In most real situations, the air leaving the drying chamber is moist and close to ambient temperature (Sodha et al., 1987; Akachuku, 1986). So, a solar chimney would not have an effect on dryer's performance unless the solar heating of the air within the chimney is significant, capable of inducing upward flow of air through the chimney. In this work the role of the solar chimney is suppressed because a constant airflow is induced by an electrical fan. However, the chimney has been designed for natural air flow, too, following the simple considerations below.

$$F_R[I_T(\tau\alpha)_e - U_{Lch}(T_{och} - T_{od})] = V_a \rho_a c_{pa}/(S * H)(T_{och} - T_{od}) \tag{20}$$

where U_{Lch} is the chimney's overall heat loss coefficient (for the same thickness of insulation: $U_{Lch} \approx U_L$), T_{och} is the temperature of the air exiting from the chimney, S is the width of the chimney (m) and H is the height of the chimney (m). Applying the momentum equation along the chimney yields:

$$\Delta P = H(\rho_a - \rho_{ch})g\frac{B}{760} - \tau_w[2(S + P)H/(S * P)] \tag{21}$$

where ΔP is the required suction pressure (N/m^2; usually $\sim$0.5 mm of water for solar chimneys, Das and Kumar, 1989), g is the acceleration of gravity (m/s^2), ρ_{ch} is the average air density in the chimney, B is the barometric pressure (mm Hg), P is the depth of the chimney (m) and τ_w is the shear stress acting on the air in contact with the chimney surface (N/m^2). The latter is given by:

$$\tau_w = \frac{1}{2}\rho_{ch} u_{ch}^2 f_{ch} \tag{22}$$

where u_{ch} is the average air velocity in the chimney ($V_a/[S * P]$) while the friction factor f_{ch} can be found using either Eq. (23) for laminar flow or Eq. (24) for turbulent flow as:

$$f_{\mathrm{ch}} = \frac{64}{\mathrm{Re}} \tag{23}$$

$$f_{\mathrm{ch}} = \frac{0.079}{\mathrm{Re}^{0.25}} \tag{24}$$

with the Reynolds number given as:

$$\mathrm{Re} = \frac{D_h \rho_{\mathrm{ch}} u_{\mathrm{ch}}}{\mu_{\mathrm{ch}}} \tag{25}$$

where D_h is the hydraulic mean diameter of the chimney defined as:

$$D_h = \frac{2S * P}{S + P} \tag{26}$$

and μ_{ch} is the average air viscosity in the chimney.

Pasumarthi and Sherif (1998) have presented a similar analysis in designing a large scale chimney for an energy plant. Ekechukwu and Norton (1995), communicated a simplified version of Eq. (21) by assuming that the pressure difference due to the buoyant pressure heat inside the chimney fully counterbalances the pressure drop due to friction losses. Putting $f_{\mathrm{ch}} = 0.003$ (for turbulent flow), the volumetric air flow rate inside the chimney is given as follows:

$$V_a = 0.113\pi D_h^2 \left[\frac{D_h g}{\rho_a}(T_{\mathrm{ch}} - T_{\mathrm{am}})\right]^{0.5} \tag{27}$$

where T_{ch} is the average temperature of the chimney; $T_{\mathrm{ch}} = (T_{\mathrm{od}} + T_{\mathrm{och}})/2$.

For given V_a, S and P, T_{och} and H can be determined solving Eqs. (20–26) or Eqs. (20), (26) and (27).

The aforementioned theoretical considerations as well as preliminary tests under certain operating conditions enabled the successful design of the novel solar dryer.

MATERIALS AND METHODS

Dryer Set-Up

The solar assisted indirect dryer discussed here, consists of a solar air collector, a heat storage cabinet, a drying chamber and a solar chimney. An outlay of the solar dryer is given in Figure 2. Black painted aluminum F2

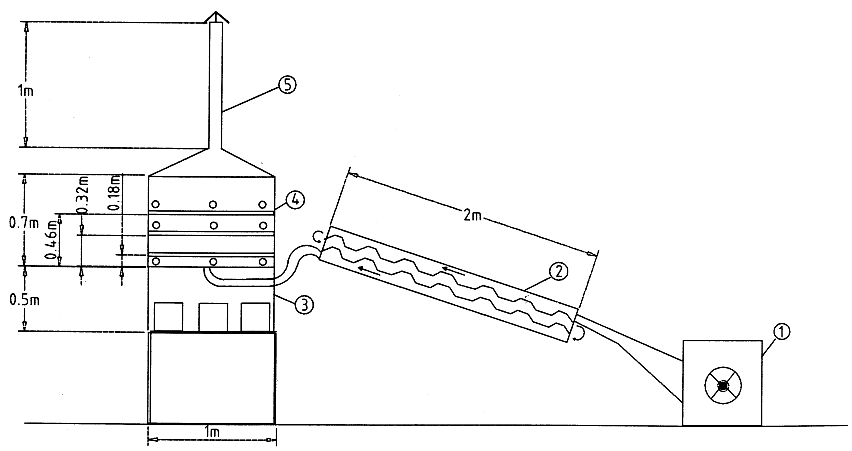

Figure 2. An outlay of the solar dryer (1. centrifugal fan 2. solar collector 3. storage cabinet 4. drying chamber 5. solar chimney). The two corrugated sheets in the solar collector with the characteristic "reverse Z" air flow path as well as the relative position of the three drawers in the drying chamber are also shown.

sheet 1.5 mm thick is used for the construction of the metallic body and walls. These walls are meant to reduce radiation heat losses due to their high solar absorptivity ($\sim$0.95) and low long wave emissivity ($\sim$0.05) (Garg, 1987). A 2.5 cm thick fiberglass layer is the insulation material wherever mentioned.

The solar collector has a parallelpiped shape with dimensions $2 \times 1 \times 0.27$ m. For the present study its longitudinal axis is oriented along the N–S direction. The collector is inclined to an angle of 37° with its back insulated. The absorbing plate consists of two aluminum corrugated sheets, 1.25 mm in thickness, placed on top of each other (Figure 2). The clearance between the sheets is 50 mm. The cover material of the collector is commercial glass 3 mm thick. A centrifugal fan (S&P, CBM-240, 0.25 kW) is connected to the lower facing end (1×0.27 m) of the collector whereas two flexible air ducts (120 mm in diameter) are connected to its higher facing end.

The heat storage cabinet has outer dimensions $1.3 \times 1 \times 0.5$ m and has insulation on the inside walls. The flexible air ducts coming out from the collector enter the cabinet and after running its interior are finally edge-pinned at the base of the drying chamber. Inside this cabinet, there are twenty-five sealed metallic containers (5 L each) filled with water and painted black to facilitate heat storage. Two hatches covered with special removable lids are constructed one at the top and the other at the bottom of the storage cabinet. These hatches are to be left open during the night operation of the dryer.

The drying chamber has $1.3 \times 1 \times 0.7\,\mathrm{m}$ outer dimensions with insulation at the inside walls. Inside the drying chamber three drawers are inserted, upon which the products to be dried are placed. The relative position of these drawers is depicted in Figure 2. The bottom drawer (drawer D_1) is placed 0.18 m above the drying chamber's base (hot air's entry point). The middle drawer (drawer D_2) is located 0.32 m and the top drawer (drawer D_3) 0.46 m above the chamber's base, respectively. The bottom of each drawer comprises of two screens—a plastic one and a very thin metallic one—placed on top of each other. Along and across each side wall of the drying chamber, 9 holes ($d = 2\,\mathrm{cm}$) are drilled to accommodate rod-shaped measuring probes.

The solar chimney comprises of two parts; a trapezoid base placed right on top of the drying chamber and the chimney duct that has the shape of a narrow parallelpiped. The chimney's duct measures externally $0.73 \times 1 \times 0.12\,\mathrm{m}$, and its front side is a commercial glass 3 mm thick. The interior of the trapezoid section is insulated, whereas the chimney duct has insulation at the outer surfaces (rear and sides). Along the two vertical narrow sides of the parallelpiped's section ($1 \times 0.12\,\mathrm{m}$), five holes ($d = 12\,\mathrm{cm}$) are opened, at equal distances from each other, to facilitate the insertion of measuring probes. A V-shaped aluminum cap (34 cm wide) is placed at the top of the chimney to protect the dryer from rain and other foreign objects. Between the chimney and the cap there is a clearance of 19 cm to allow warm humid air to exit freely from the dryer. The chimney duct is capable to stand at various inclinations between 90° (vertical) and 30°. In this study only the vertical position is used.

Method of Operation

Ambient air is sucked by the centrifugal fan through an intermediate funnel and enters the solar collector where it preheats. The funnel has internal guiding fins to uniformly distribute the air over the width of the collector. Air runs three passes inside the solar collector in a "reverse Z" flow path, Figure 2. The air leaving the collector is pre-heated to approx. 10–$20^\circ\mathrm{C}$ above ambient temperature and after running through the heat storage cabinet it emerges at the base of the drying chamber. The section of the ducts connecting the solar collector to the heat storage cabinet is thermally insulated. On the other hand, the ducts section running the interior of the storage cabinet is left bare (without insulation). Thus, an appreciable amount of heat is transferred (and stored) from the hot surface of the bare ducts to the metallic containers in the storage cabinet. The hot air exiting from the flexible ducts at the bottom of the drying chamber, disperses over the available space of the chamber and as a result its velocity is drastically reduced. This is important if uniform and slow drying of a wet product must be achieved. After traveling inside the drying chamber (around and through the drawers) air enters the solar chimney from where it eventually escapes to the environment.

During the night, when the solar collector and the fan are out of operation, it is imperative to avoid raising of the humidity inside the drying chamber since products already dried to some extent are much more susceptible to re-hydration. For this, the top and bottom hatches of the heat storage cabinet remain open throughout the night until the collector is put in operation again the next day. During these hours, the fresh air that enters from the bottom hatch (base of storage cabinet) allows the dryer's aeration by natural convection along the dryer. This rising air absorbs heat from the water containers in the storage cabinet and as it warms up its relative humidity goes down allowing the dehydration of the products to continue even at a much slower pace.

It must be mentioned that in this work the air flow inside the dryer is always dictated by the centrifugal fan in an effort to maintain a constant flow rate for all runs. This was done in order to reduce the experimental variables and so simplify the assessment of the dryer's performance. In addition, the use of the fan suppresses the role of the solar chimney in assisting airlift. However, in rural applications it may be preferable not to use an electrical fan but let the solar chimney alone drag the hot air through the dryer. In such a case, the solar collector will have to stand at a lower position than the rest of the dryer so as to create a positive head with respect to the dryer.

Materials and Measurements

Carpentry sponge made of polyurethane foam (MultiFoam Inc.) 1 cm thick is used as a reference drying material. This sponge has a spatially uniform porosity ($\varepsilon_{\mathrm{ave}} \approx 0.85$) with narrow pores ($d_{\mathrm{ave}} \approx 0.5$ mm) which upon hydration produces a uniform moisture content across the material. Yet, it is a non-hygroscopic material and so it can be dried completely (i.e. zero moisture content) which is clearly not the case with most agricultural products. However, the use of carpentry sponge facilitates the evaluation of the dryer's performance because it allows highly reproducible initial hydration and subsequent dehydration patterns. In order to get the sponge initially saturated with water it is necessary to soak it in water and then squeeze-dry it at least twice prior to its final wetting and placement in the drying chamber. The experiments are divided into three categories: (a) with no material inside the drying chamber (empty trays) (b) with a single large sponge piece covering the entire surface area of each drawer and (c) with eighteen individual small sponge pieces ($150 \times 215\,\mathrm{mm}$) placed next to each other to cover the area of each drawer. The air flow rate is maintained essentially constant in all runs at $200\,\mathrm{m^3/h}$.

In addition to loss-in-moisture measurements, the velocity, temperature and relative humidity of the air inside the dryer are also measured. For this, a Tri-Sense electronic microprocessor (Cole-Parmer) is employed. The microprocessor is equipped with separate probes for measuring: (1) temperature ($\pm 1^\circ$) and air velocity ($\pm 0.1\,\mathrm{m/s}$), (2) temperature ($\pm 1.5^\circ$) and relative humidity ($\pm 2\%$) and (3) two simultaneous temperatures at two different locations ($\pm 0.4^\circ$). Values in parentheses denote the claimed accuracy of measurements while the resolution is an order of magnitude better. For measurements in the interior of the drying chamber, the measuring probes are inserted through the holes opened at the two side walls of the chamber. The position of these holes divides the drying chamber into three horizontal, (A), (B), (C) and three vertical virtual planes, (a), (b), (c). These virtual planes are shown in Figure 3. It must be mentioned that plane (A) is **F3**
just below drawer D_1, plane (B) is between drawers D_2 and D_3 and plane (C) is just above drawer D_3.

The experiments are carried out during selected days in August and September 2000. Total solar radiation on a horizontal plane is measured simultaneously with ambient temperature, relative humidity, wind speed and wind direction at the meteorological station in TEI. Irradiation data are collected using an Eppley Precision Pyranometer (model PSP), which was calibrated at the beginning of the measuring period. The estimated overall error in solar irradiance measurements—including calibration, measurement, digitization and data handling—is less than 3%. All data are integrated over 1 h intervals. The experiments reported are mainly performed during clear sky days but a few runs are also conducted during the days that were cloudy or even rainy.

RESULTS

Three separate full day tests are carried out with an empty drying chamber, i.e. without the presence of sponge on the trays. Here, data of just one test (August 23rd) are presented since all runs showed an essentially similar behavior. Temperature variation inside the empty drying chamber is depicted in Figure 4 regarding the horizontal plane (A). The temperatures **F4**

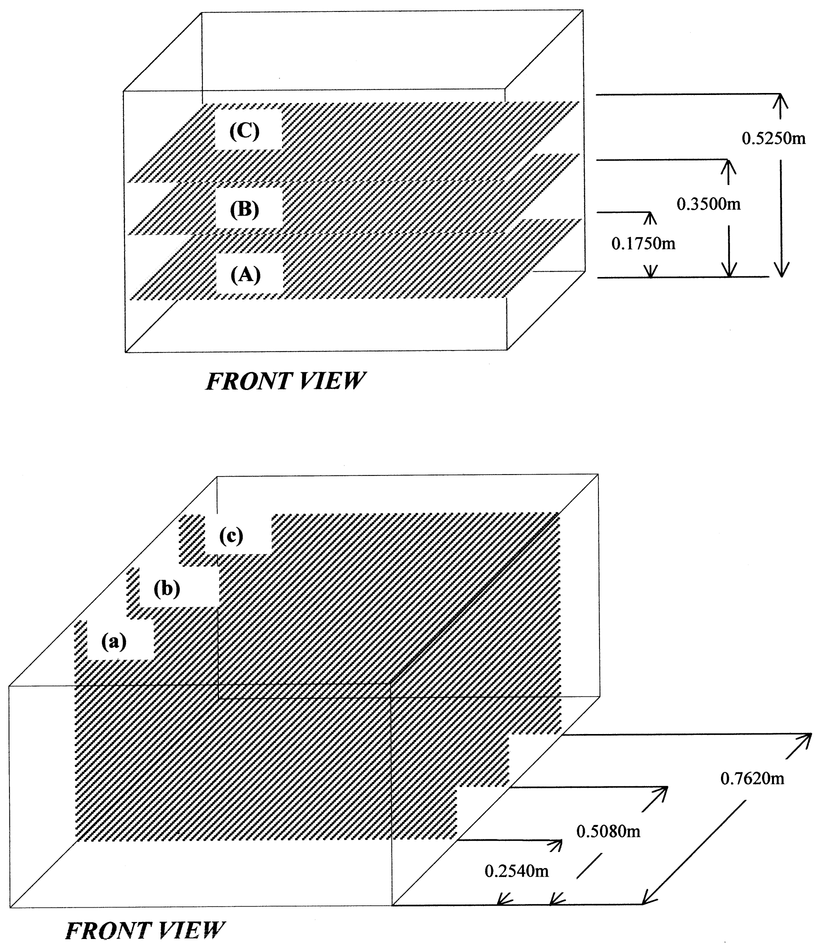

Figure 3. A layout of the virtual measuring planes inside the drying chamber.

at the other two horizontal planes vary in a similar manner. In this figure, the three vertical planes (a), (b), (c), are shown as a parameter. To show the effect of the temporal variation of solar irradiance, measurements obtained between 14:30–15:00 are presented for the left side of the chamber and between 17:00–17:30 for the right side of the chamber. Higher temperature values are presented for the left side of the drying chamber, which is attributed to the relative position of the sun at the time of measurements (14:30–15:00). The temperatures at the right side of the chamber interior

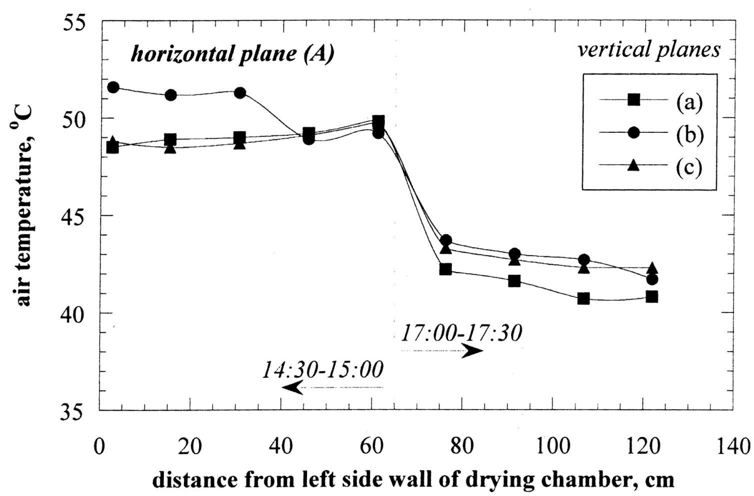

Figure 4. Temperature variation at the horizontal plane (A) inside the empty drying chamber (run on August 23rd).

are lower by ~5–10°C since they are measured at a later time of the day (17:00–17:30). Thus, the temperature distribution inside the drying chamber is a function of the hour of the day (in fact, of the relative position of the sun in the sky).

Typical air velocity charts for the same run, obtained at the three horizontal planes, i.e. (A), (B), (C), are shown in Figure 5. As one might **F5** have expected, at the lower horizontal plane (A) and just above the exit of the two air ducts (plane (b)), air velocity attains higher values, while for all other positions it is substantially less. Moving towards the solar chimney, i.e. planes (B) & (C) (Figures 5b and c respectively), the high velocity values at plane (b) drop drastically and become gradually more uniform across the drying chamber.

Three experiments are carried out with pre-wetted large sponges placed inside the drying chamber, one for every drawer. Again, results from one run are presented (September 11th) since the other runs exhibit similar trends. For this particular run the sponge is introduced in the dryer at noon (12:00). Table 2 presents hourly average values of total radiation on **T2** a horizontal plane, ambient temperature and relative humidity during the hours of this test.

With regard to temperature variation, at the level of plane (A) relatively higher temperatures are observed compared to planes (B) and (C) (Figure 6, measurements are obtained around 14:00). Moreover, the **F6**

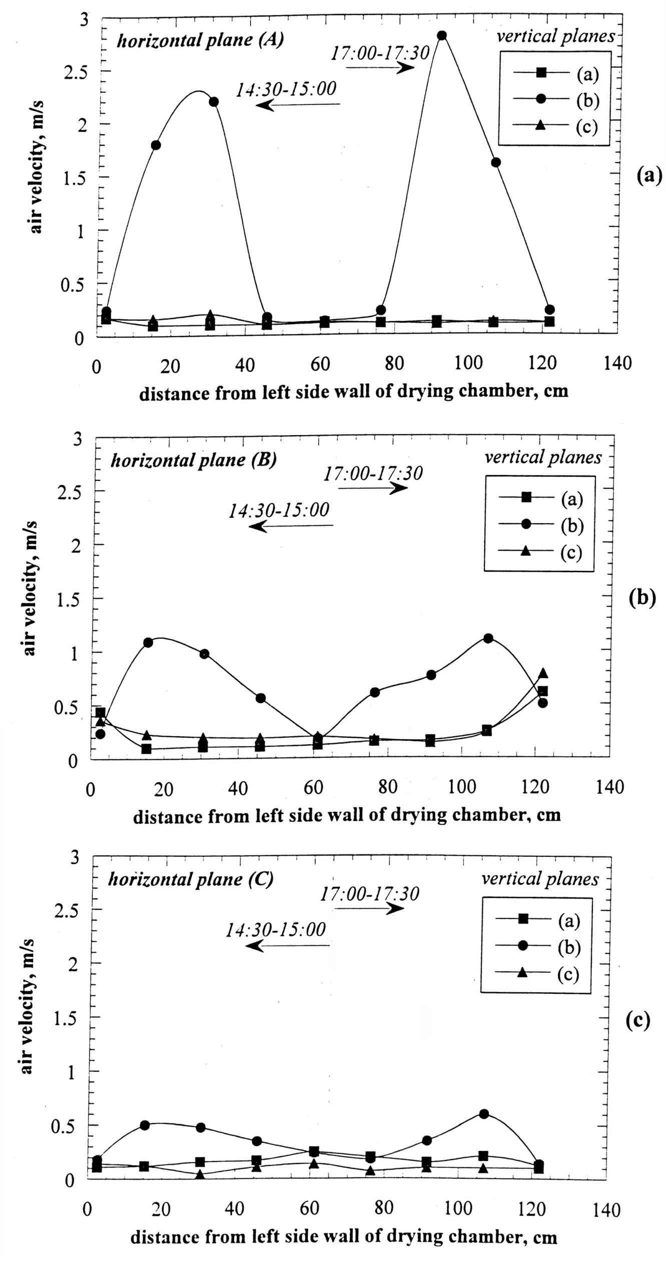

Figure 5. Typical air velocity distribution charts at there horizontal planes (A), (B), and (C), in an empty drying chamber (run on August 23rd).

Table 2. Hourly Average Total Radiation on a Horizontal Plane, Ambient Temperature and Relative Humidity During one Representative Experimental Day (Run of September 11th)

	Hour of Day	Hourly Average Total Radiation on Horizontal Plane kW/m^2	Ambient Temperature °C	Ambient Relative Humidity %
September 11th	12:00	0.727	24.4	62
	14:00	0.894	27.4	48
	16:00	0.606	29.0	44
	18:00	0.091	27.8	47
	20:00	0.015	26.4	51

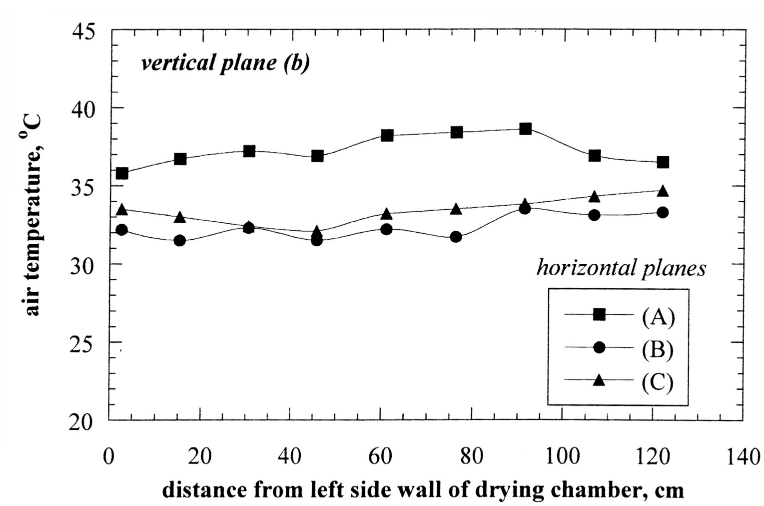

Figure 6. Temperature distribution at the vertical plane (b) inside the drying chamber (run on September 11th).

values of planes (B) and (C) appear to be roughly constant across the chamber. Figure 6 refers only to vertical plane (b). However, a qualitatively similar trend is also observed at the other two vertical planes. Comparing Figure 6 with Figure 4 shows that the temperature of the air inside the drying chamber is lower under drying conditions, as expected.

Air velocity variation inside the drying chamber at the horizontal planes (A) and (C) is given in Figure 7 (plane (B) displayed a similar F7

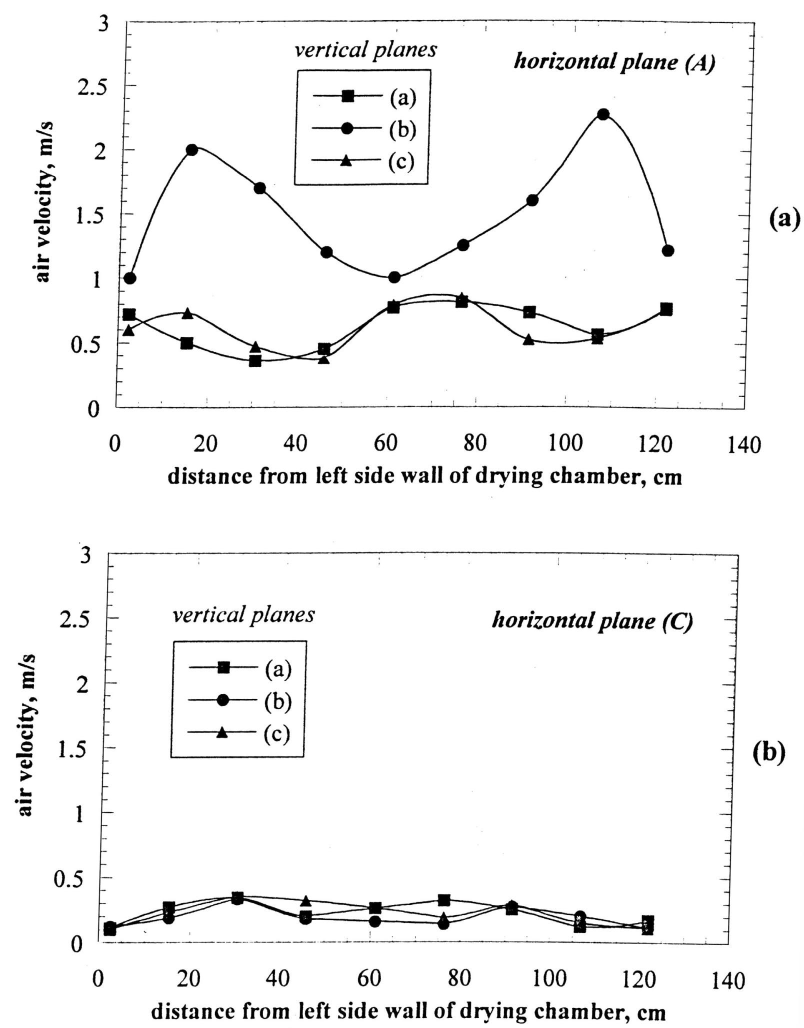

Figure 7. Air velocity distribution at the horizontal planes (A) and (C), inside the drying chamber bearing pre-wetted large sponges, one for every drawer (run on September 11th).

behavior with plane (C)). Air velocity at the lower horizontal plane (A) is relatively higher compared to values obtained at plane (C) (i.e. near the chamber top). As in Figure 5, air velocity at the vertical plane (b), attains its higher values just above the two air ducts while in most other measuring

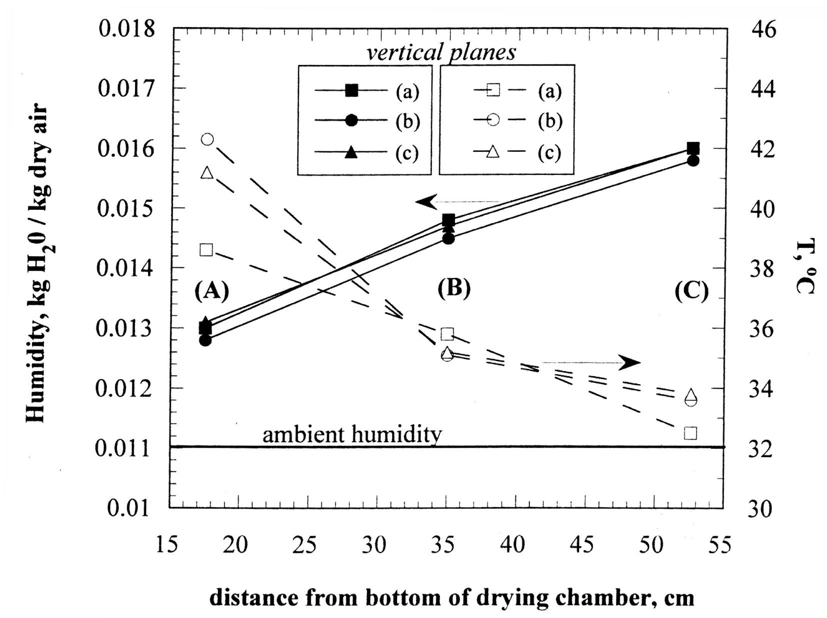

Figure 8. Air humidity and temperature variation with respect to vertical distance from the drying chamber bottom.

spots the velocity values are significantly lower and comparable with each other. It is noteworthy, though, that these lower values are in general higher than the respective values in Figure 5. Thus, it is apparent that the presence of solid material on the trays enhances the dispersion and uniformity of air flow inside the drying chamber.

Figure 8 displays the variation of air humidity and temperature with respect to vertical distance from the bottom of the drying chamber. Ambient humidity is included in the graph for comparison. Measurements are taken 3 h after the introduction of the wet sponges to the dryer. It is apparent that humidity increases while temperature decreases with vertical distance, owing to evaporation of water from the wet material. F8

The drying curves obtained during the run of September 11th are shown in Figure 9. The shape of the curves for all drawers is typical of drying a non-hygroscopic material (Garg, 1987). As one might have expected, drawer D_1, i.e. the one placed nearer to the two air ducts, exhibits the most rapid drying. After only a 4-h period, the product at this drawer is almost completely dried, in contrast to drawers D_2 and D_3 where 6 and 7-h periods are needed respectively for a complete drying. F9

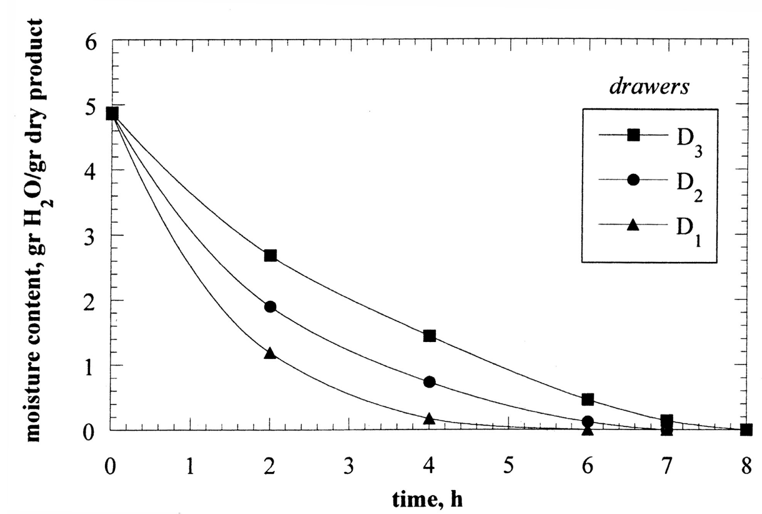

Figure 9. Drying curves plotted as moisture content on a dry basis vs. time (run on September 11th).

Employing Eq. (19), the drying efficiency for the first two hours is estimated around 45%$\pm$5% for all runs while for the subsequent two hours of drying it falls approximately at half of this value. As the water content of the material reduces and drying likely moves from the constant rate to the falling rate period, the efficiency of the dryer drops in spite of the fact that the heat offered by the collector does not vary markedly. This is so because during the falling rate period the moisture movement inside the solid dictates the drying rate. In practice, one way to circumvent the problem and increase the efficiency during the falling rate period is by increasing the temperature of the air entering the drying chamber. This can be done by e.g., lowering the air-flow rate (Perry and Chilton, 1973). Yet, care should be taken in real applications not to increase the temperature of the air beyond a certain value in order to avoid the product's quality degradation.

The performance of the dryer is checked also under adverse weather conditions. At a Mediterranean climate it is quite usual to encounter sporadic cloudy sky conditions with chances of a rainfall of short duration. Herein, the results of such a run performed on September 26th are presented. For this run the material was introduced in the dryer at 10:30 a.m. At around 12:00 dense clouds begun to cover the sky and the weather climaxed at 13:00 with a mild shower. At 13:30 the rain stopped but the sky was intermittently covered until 14:30 when the sky became clear again.

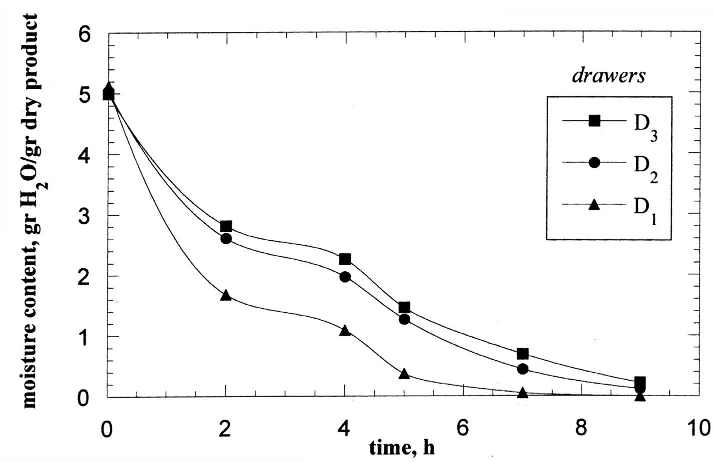

Figure 10. Drying curves under adverse weather conditions (run on September 26th).

The effect of the weather conditions is clearly depicted in Figure 10 where an anomaly (leveling-off) in the drying curve is detected during the overcast period and which delayed the drying process. It is noteworthy that despite the adverse conditions during this period, the moisture content of the solid continues to decrease even though at a much lower rate. Perhaps this is partly due to the increased heat capacity of the dryer's metallic body which, for a short period of time, can provide heat to compensate for the absence of solar radiation. Furthermore, the drying rates and drying efficiencies calculated for the three drawers are quite similar to the clear sky experiment on September 11th. F10

Finally, an experiment (starting September 8th—ending September 9th) is presented where individual small sponge pieces are used to cover the trays of the dryer. The aim for this test is to identify favorable and unfavorable spots on the drawers as regards drying efficiency and also investigate the performance of the dryer during the night operation. During the night hours the electrical fan is turned off and the hatches at the top and bottom of the heat storage cabinet are left open to allow air natural convection inside the dryer.

Similar results with the single sponges' experiment are obtained regarding temperature, air velocity and relative humidity (Figures 6–8). What is perhaps of greater significance is the drying performance. The drying curves for two opposing limiting spots (as regards drying rate) on the trays of the drawers are given in Figure 11. In particular, Figure 11a F11

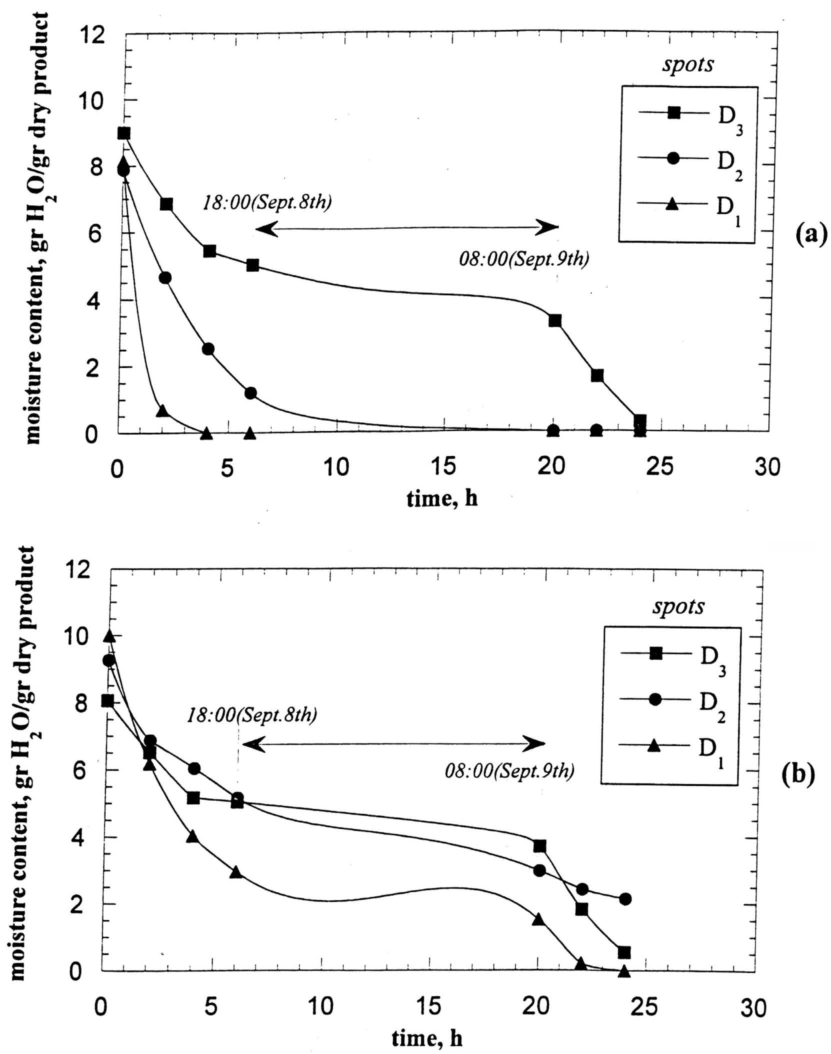

Figure 11. Drying curves for two opposing limiting spots on the drawers: (a) favorable drying and (b) unfavorable drying.

displays curves for all three drawers measured at the spot right above the air ducts, where the conditions are among the most favorable ones (fast drying). On the other hand, Figure 11b presents curves obtained near the front wall of the drying chamber which is among the least favorable ones. In fact, only the spots right above the exit of the ducts (for drawer D_1) exhibit a markedly higher drying rate. The rest behave more or less like the spot in Figure 11b. This means that, with the exception of the spots above the air ducts (for drawer D_1), there is an appreciable uniformity inside the dryer but also suggests that a modification of the exit section of the ducts must be imparted to prevent the direct ejection of hot air to the bottom of drawer D_1. Of particular interest, is the behavior of the system over the night. It is clearly seen that not only the sponges' moisture content does not increase but continues to decrease even though at a slower rate. The benefit from the use of the heat storage cabinet is evident. A similar finding was also obtained by Aboul-Enein et al. (2000) when studying the night operation of a solar-assisted drying system.

CONCLUSIONS

In this study, the performance of a prototype tray dryer equipped with a solar air collector, a heat storage cabinet and a solar chimney is described. The dryer is easy to construct and operate and can be implemented at low cost. Considering the different weather conditions tested (sunny, cloudy or rainy), the drying process reached full completion in all tests at a reasonable rate of dehydration. Experimentation over the night, without the use of the centrifugal fan, confirmed the system's good performance regarding the usefulness of the heat storage cabinet since the products' water content continued to decrease although at a lower rate. Fairly promising results were obtained regarding the solar dryer's efficiency. The latter can be improved by properly adjusting the flowrate and temperature of the air entering the drying chamber. With regard to drying uniformity throughout the drying chamber special attention should be given to products placed at the lower drawer just above the entry points of the two flexible air ducts where excessively faster drying occurs. Periodic agitation of the solids in the lower drawer, exchange of drawer's position or a new design of the air exit section from the ducts may alleviate this problem.

NOMENCLATURE

A	Area (m^2)
B	Barometric pressure (mm Hg)
c_p	Average heat capacity (kJ/kgK)
D_h	Hydraulic mean diameter of the chimney (m)
f	Friction factor

F_R	Collector heat removal factor
g	Acceleration of gravity (m/s^2)
G_{sc}	Solar constant (1367 W/m^2)
H	Chimney height (m)
I	Total solar radiation on horizontal plane (kJ/hrm^2)
I_b	Beam (or direct) radiation (kJ/hrm^2)
I_d	Diffuse radiation from the sky (kJ/hrm^2)
I_o	Extraterrestrial radiation on an horizontal plane (kJ/hrm^2)
I_t	Insolation rate per unit area on the collector's tilted plane (kJ/hrm^2)
k_T	Clearness index
m	Solid's moisture content (kg H_2O/kg dry solid)
n	Day of the year (1 to 365)
P	Chimney depth (m)
R_b	Ratio of beam radiation on the tilted surface to that on the horizontal plane
Re	Reynolds number
r_g	Diffuse reflection of the surroundings
S	Chimney width (m)
Sot	Solar time (min)
Stt	Standard time (min)
t	Drying period (h)
T	Temperature (°C)
u	Average air velocity (m/s)
U_L	Collector's overall heat loss coefficient (kJ/hrm^{2}K)
U_{Lch}	Chimney's overall heat loss coefficient (kJ/hrm^{2}K)
V	Volumetric flow rate (m^3/h)
W	Weight of dry solid (kg)
y	Absolute humidity of air (kg H_2O/kg dry air)

Greek Letters

α	Absorbance
δ	Declination (angular position of the sun at solar noon)
ΔP	Suction pressure (kg/ms^2)
λ	Average latent heat of water (kJ/kg)
μ	Average air viscosity (kg/ms)
ρ	Average density (kg/m^3)
ρ_o	Air density $T = 273$ K (=1.293 kg/m^3)
τ	Transmittance
τ_w	Shear stress acting on the air in contact with the chimney surface (kg/ms^2)

ϕ	Latitude of the site (angular location from the equator) AQ2
ω	Hour angle (angular displacement of the sun east or west from local meridian, in deg)

Subscripts

a	Air
am	Ambient
c	Collector
ch	Chimney
f	Final
i	Initial
od	Exit from drying chamber
oc	Exit from collector
och	Exit from chimney
p	Collector's plate
s	Solid
w	Water

REFERENCES

Aboul-Enein, S.; El-Sebaii, A.A.; Ramadan, M.R.I.; El-Gohary, H.G. Parametric Study of a Solar Air Heater with and without Thermal Storage for Solar Drying Applications. Renewable Energy **2000,** *21*, pp. 505–522.

Akachuku, A.E. Solar Kiln Dryers for Timber and Agricultural Crops. Int. J. Ambient Energy **1986**, *7*(2), pp. 95–101.

Arinze, E.A.; Schoenau, G.J.; Sokhansanj, S. Design and Experimental Evaluation of a Solar Dryer for Commercial High-quality Hay Production. Renewable Energy **1999**, *16*, pp. 639–642.

Bala, B.K.; Mondal, M.R.A. Experimental Investigation on Solar Drying of Fish Using Solar Tunnel Dryer. Drying Technology **2001**, *19*(2), pp. 427–436.

Bansal, N.K.; Garg, H.P. Solar Crop Drying, Vol. 4. In *Advances in Drying*, Mujumdar, A.S., Ed.; Hemisphere Publishing: New York, 1987.

Barbosa-Canovas, G.V.; Vega-Mercado, H. *Dehydration of Foods: Other Methods of Dehydration of Foods and Packaging Aspects*, Chapman and Hall: New York, 1996.

Das, S.K.; Kumar, Y. Design and Performance of a Solar Dryer with Vertical Collector Chimney Suitable for Rural Application. Energy Convers. Mgmt. **1989**, *29*(2), pp. 129–135.

Duffie, J.A.; Beckman, W.A. *Solar Engineering of Thermal Processes*, 2nd edition, John Wiley and Sons: New York, 1991.

Ekechukwu, O.V.; Norton, B. Design and Measured Performance of a Solar Chimney for Natural Circulation Solar Energy Dryers. J. of Solar Energy Engineering, Transaction of the ASME **1995**, *118*, pp. 69–71.

Ekechukwu, O.V.; Norton, B. Effects of Seasonal Weather Variations on the Measured Performance of a Natural-Circulation Solar-Energy Tropical Crop Dryer. Energy Conversion and Management **1998**, *39*, pp. 1265–1276.

Ekechukwu, O.V.; Norton, B., Review of Solar-Energy Drying Systems II: An Overview of Solar Drying Technology. Energy Conversion and Management **1999**, *40,* pp. 615–655.

Esper, A.; Muhlbauer, W. Solar Drying—An Effective Means of Food Preservation. Renewable Energy **1998**, *15*, pp. 95–100.

Garg, H.P. Solar Food Drying, Vol. 3. In *Advances in Solar Energy Technology. Heating, Agricultural and Photovoltaic Applications of Solar Energy*, D. Reidel Publishing Co.: Dordrecht, Holland, 1987.

Imre, L.; Fabri, L.; Gemes, L.; Hecker, G. Solar Assisted Drier for Seeds. Drying Technology **1990**, *8*(2), pp. 343–349.

Imre, L. Solar Drying. In *Handbook of Industrial Drying*, Mujumdar, A.S., Ed.; Marcel Dekker, Inc.: New York and Basel, 1987; Chap. 11.

Jansen, T.J. *Solar Engineering Technology*. Prentice-Hall, Inc.: New Jersey, 1985; Chap. 7.

Karapantsios, T.D.; Hatzimoisiadis, K.A.; Balouktsis, A.I. Estimation of Total Atmospheric Pollution Using Global Radiation Data: Introduction of a Novel Clear Day Selection Methodology. Renewable Energy **1999**, *17*, pp. 169–181.

Lallas, F.P.; Pissimanis, F.K.; Notaridou, V.A. Methods of Estimation of the Intensity of Solar Radiation on a Tilted Surface and Tobulated Data for 30°, 45° and 60° in Greece. Tech. Ch.-B **1982**, *2*, pp. 129–180 (in Greek). **AQ1**

Liu, B.Y.H.; Jordan, R.C. The Long Term Average Performance of Flat Plate Solar Energy Collectors. Solar Energy **1963**, *7*, pp. 53–74.

Oosthuizen, P.H. A Numerical Study of the Performance of Natural Convection Solar Rice Dryers, *Proc. Fifth International Drying Symposium DRYING'86*, Mujumdar, A.S., Ed.; Hemisphere: New York, 1987; pp. 670–677.

Pasumarthi, N.; Sherif, S.A. Experimental and Theoretical Performance of a Demonstration Solar Chimney Model—Part I: Mathematical Model Development. Int. J. Energy Res. **1998**, *22*, pp. 277–299.

Perry, R.H.; Chilton, C.H. *Chemical Engineer's Handbook,* 5th Edition; McGraw-Hill: New York, 1973.

Pratoto, A.; Daguenet, M.; Zeghmati, B. Sizing Solar-Assisted Natural Rubber Dryers. Solar Energy **1997**, *61*(14), pp. 287–291.

Ratti, C.; Mujumdar, A.S. Solar Drying of Foods: Modeling and Numerical Simulation. Solar Energy **1997**, *60*(3/4), pp. 151–157.

Sodha, M.S.; Bansal, N.K.; Kumar, K.; Bansal, P.K.; Malik, M.A.S. *Solar Crop Drying*, Vol. 1, CRC Press: FL, 1987.

Sukhatme, S.P. *Solar Energy: Principles of Thermal Collection and Storage*, Fifth Reprint, Tata McGraw-Hill: New Delhi, 1990. **AQ3**

Tiris, C.; Ozbalta, N.; Tiris, M.; Dincer, I. Experimental Testing of a New Solar Dryer. International Journal of Energy Research **1994,** *18*, pp. 483–491.

Tsamparlis, M. Solar Drying for Real Applications. Drying Technology **1990**, *8*(2), pp. 261–285.